AIAA JOURNAL
Vol. 41, No. 9, September 2003

Trailing-Edge Cavity Afterbodies for Linear Plug Nozzle Engines

Menko E. N. Wisse* and Willem J. Bannink†
Delft University of Technology, 2629 HS Delft, The Netherlands

Linear plug nozzles have been receiving more attention since the development of the single stage to orbit reusable launch vehicle. It is well known that supersonic external flows cause a degradation of the plug nozzle performance. To minimize this degradation, different kinds of afterbody shapes can be chosen. Instead of boattail shapes, the present study concerns the use of (ventilated) trailing-edge cavities. Various models of the afterbody have been used to investigate numerically performance with an external flow at a Mach number of $M_\infty = 2$. Navier–Stokes equations provided with a Baldwin–Lomax turbulence model and a Degani–Schiff correction were used for these calculations. For all of these models, the effects of increasing or decreasing pressure ratio have been taken into account, as well as the use of different truncations of the plug nozzle.

Nomenclature

A	=	area
A^*	=	sonic area
L	=	full plug length
M	=	Mach number
p	=	pressure
T	=	temperature
X, Y	=	coordinates
γ	=	ratio of specific heats
θ_t	=	tilt angle of the throat

Subscripts

c	=	chamber conditions
d	=	design conditions
e	=	exit conditions
nb	=	nozzle base
nr	=	nozzle ramp
t	=	throat conditions
t_∞	=	freestream stagnation conditions
vb	=	vehicle base
∞	=	freestream static conditions

Introduction

THE key demands on future space transportation systems are the reduction of Earth-to-orbit launch costs in conjunction with an increase in launcher reliability and operational efficiency. A possible approach to provide cheaper access to space, relies on the use of a single stage to orbit reusable launch vehicle (RLV). Such an RLV will reduce the costs to get payload into space to 1/10th of the present costs. One of the biggest challenges to achieve this, is to develop a lightweight propulsion system that has an optimum performance during the entire launch trajectory. One of the most promising candidates for such a system is the linear plug nozzle engine.[1]

A lot of research have been performed since the 1950s.[2–12] In contrast to the other nozzle concepts, plug nozzles possess beneficial properties that satisfy the requirements of minimizing vehicle weight and maximizing engine thrust.[2]

First, the altitude adaptation property gives the plug nozzle an important performance advantage with respect to a bell nozzle by self-adjusting the effective nozzle area ratio. At low altitudes (relatively high ambient pressures) the efficiency in thrust can be considerably higher than that of a bell nozzle. In this underexpanded flow regime, boundary-layer separation occurs in the classical bell nozzles divergent section, which can induce strong side loads along with a significant drop in the nozzle efficiency.[1]

Second, a better utilization of the vehicle base is accomplished due to the following features. First, the plug nozzle reduces the harmful drag producing base area. Second, because almost the entire vehicle base can be utilized as nozzle exit area, very large nozzle area ratios may be obtained, which is to the benefit of a higher thrust performance in vacuum. Third, the thrust load is distributed over a large effective vehicle base area occupied by the plug, offering a possibility to reduce the weight of the thrust-generating structure. In contrast, the bell nozzle is subject to a point source load.

However, plug nozzles should be studied in conjunction with the vehicle forebody because local external flow variations caused by the forebody affect the efficiency of the plug nozzle. The interaction between external flow and the expanding exhaust jet along the plug contour may change the beneficial concept of its altitude compensating capabilities. In subsonic flight the jet will entrain the ambient flow, and in transonic and supersonic flight the external flow over the vehicle expands into the vehicle base region. This induces a decrease in vehicle base pressure, causing the jet to overexpand, with a resultant dramatic degradation of the plug nozzle performance.[6]

This degradation can be minimized by choosing different kinds of afterbody shapes. Boattail shapes have been subject of investigation in the work of Wasko.[12] The present study concerns the use of a (ventilated) trailing-edge cavity, which Nash[13] previously used for base drag reduction. Its task is to prevent the external flow from interacting with the jet. The ventilation slit is expected to increase the static pressure in the vehicle base wake. The effect of this afterbody shape on the plug nozzle performance is investigated for different plug truncations and pressure ratios (p_c/p_∞) by means of a Navier–Stokes code. This study is only a first attempt to find out whether the use of this (ventilated) trailing-edge cavity is capable of increasing the plug nozzle performance.

The paper will cover the following topics. First, the plug nozzle geometry will be discussed. Then, a short description of the code will be given including the solution procedure, followed by a description of the plug nozzle flow physics. Subsequently, the grid implementation and boundary conditions will be treated. The last paragraphs will be devoted to the discussion of the results and the conclusions.

Geometry

The symmetrical model, shown in Fig. 1, is the same model which has been used in previous investigations.[6,7] It has an overall height of

Received 13 March 2001; presented as Paper 2001-1892 at the AIAA/NAL–NASDA–ISAS 10th International Space Planes and Hypersonic Systems and Technologies Conference, Kyoto, Japan, 24–27 April 2001; revision received 2 October 2001; accepted for publication 29 April 2003.

*Research Fellow, Department of Aerospace Engineering, Kluyverweg 1. Member AIAA.

†Associate Professor, Department of Aerospace Engineering, Kluyverweg 1.

67.23 mm. The nozzle throat is sonic with a throat area of $A_t = 4$ mm and a tilt angle $\theta_t = 67.84$ deg; it corresponds to the Prandtl–Meyer angle to deflect the flow at a ratio of specific heats of $\gamma = 1.4$ to the horizontal direction resulting in the design Mach number of $M_d = 4.16$ and a design pressure ratio of $p_c/p_\infty = 188$. The corresponding ratio of exit area to throat area at design conditions is $A_d/A_t = 12.35$. The plug nozzle is designed following the method of Angelino.[14] The plug is a solid boundary following a streamline from the Prandtl–Meyer expansion (simple wave) starting at the sonic nozzle throat. A full plug, that is, with a contour from the starting point of the plug ramp (throat) to freestream flow direction, would have a plug length of $L = 203.2$ mm. Plug lengths truncated to 20 and 40% of the full plug length were used.

As in previous the study,[6] the model was exposed to an external flow with $M_\infty = 2$ for various pressure ratios (p_c/p_∞). Models 1 and 2 are, respectively, a 20 and a 40% symmetrical model. Model 3 is a 20% model extended with a 100-mm-long and 1-mm-thick cavity tail. This cavity tail is ventilated in models 4 and 6 for a 20% model and in model 5 for a 40% model. Models 4 and 5 have a 1-mm slit, and model 6 has a 2-mm slit. These models are presented in Table 1.

Numerical Tools

Numerical simulations of the viscous (turbulent) flows over the plug geometries were performed using a Navier–Stokes code developed at Delft University of Technology.[15] The code is based on a cell-centered finite-volume descretization. It is provided with second-order accurate upwind discretization according to the flux-vector splitting of Van Leer. Higher-order spatial discretizations are obtained with MUSCL, an interpolation technique with a Van Albada limiter to suppress spurious oscillations at discontinuities. The viscous terms are discretized using central differences.

The system of nonlinear discretized equations is solved with an implicit line Gauss–Seidel method within an efficient nonlinear multigrid solution procedure. Within this multigrid, the solutions at the different grid levels have been smoothed by an implicit relaxation method.

For the calculations, a Baldwin–Lomax turbulence model[16] was used with a Degani–Schiff correction.[17] The algebraic Baldwin–Lomax turbulence model is accurate for steady flows with little or no separation, it is, however, easy to use and economic. The Degani–Schiff correction is capable of choosing the appropriate length scale for these separated flows. The turbulence generation process is dominated by the attached boundary layers, rather than the vortical flows. The Degani–Schiff correction defines this length scale and, therefore, simulates the eddy viscosity in the base flow and the shock wave–boundary-layer interaction region more properly. Its capabilities for these kind of flows have already been proven.[6]

Table 1 Test models used for computations

Model	Truncation, %	Cavity Tail	Slit, mm
1	20		
2	40		
3	20	•	
4	20	•	1
5	40	•	1
6	20	•	2

Plug Nozzle Flow Physics

Altitude Adaptation

The attractive feature of the plug nozzle mentioned in the Introduction is illustrated in Fig. 2. Hagemann et al.[9] divide the flow physics into three major categories. For pressure ratios lower than the design pressure ratio of a plug nozzle (Fig. 2a), the flow primarily expands along the central plug body to the ambient pressure p_∞. Only the first part of the nozzle ramp acts as an expansion contour down to the point where the last right running characteristic, which feels the ambient pressure, meets the ramp. When this characteristic is passed, the flow is adapted to the ambient pressure and is inclined toward the centerline. Downstream of this characteristic, the slope of the ramp, designed as a clean expansion contour at its design pressure ratio, deviates the uniform flow outward, thereby generating compression waves that run toward the outer freestream shear layer. The compression waves are reflected by the shear layer as expansion waves, deflecting the jet upward. The expansion waves are reflected on the ramp as expansion waves that are reflected by

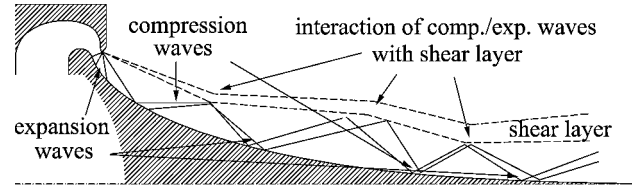

a) Underexpanded condition

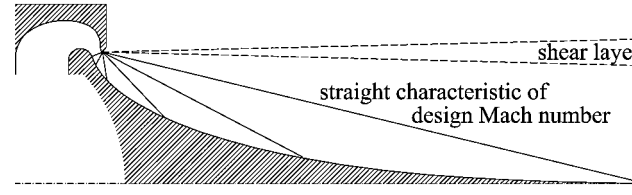

b) Design condition

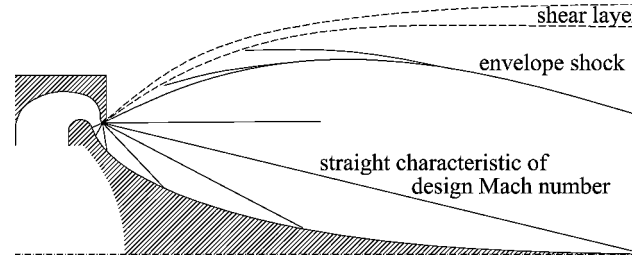

c) Overexpanded condition

Fig. 2 Flow phenomena on a plug with full length at different pressure ratios p_c/p_∞.

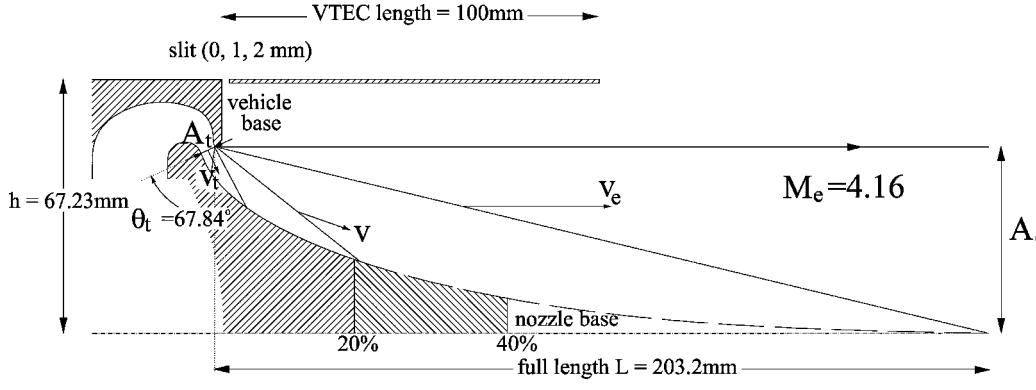

Fig. 1 Plug nozzle model.

the shear layer as compression waves again. In this way, a system of recompression waves/shocks and expansion waves adapts the exhaust flow to the ambient pressure and to the plug nozzle symmetry line. In general, the waves reflect on the ramp in like manner and on a shear layer in an opposite manner as is also the case on the nozzle base shear layer. At the design pressure ratio (Fig. 2b), the straight characteristic with the design Mach number corresponds to a flow direction parallel to the centerline, and thus, the shear layer is also parallel to the centerline. At pressure ratios above the design pressure ratio (overexpansion) (Fig. 2c), the pressure distribution along the plug ramp remains the same as for the design pressure ratio. In this way the expanding jet is not fully used for thrust.

The altitude adaptation lies in that the plug nozzle jet is not enclosed like in the case of a bell nozzle. Its gases are expanded in such a way that the jet is always exposed to the ambient pressure. As long as the pressure ratio is below the design value, compression waves in the jet impinge on the plug ramp generating high static pressures through the recompression mentioned earlier. The plug nozzle loses its capability for further altitude adaptation beyond its design condition.

Plug Truncation

More than half of the full length plug produces almost no thrust, but it does produce shear stresses and adds weight to the system as well. From that point of view, it may be removed leaving a truncated plug. It results in a different flow and performance behavior as compared to the full length plug.[9] A base flow is established behind the truncation. This base flow phenomenon in conjunction with the plug nozzle is well described by Wisse and Bannink.[6] At lower pressure ratios, an open wake flow establishes (Fig. 3a). At a certain pressure ratio close to the design pressure ratio of the full length plug nozzle, the base flow reaches the closed form, characterized by a constant ratio of nozzle base pressure p_{nb}/p_c that is no longer influenced by the ambient pressure (Fig. 3b). This is the pressure ratio where the last right running characteristic has traveled beyond the base flow region. For this pressure ratio and higher pressure ratios, the pressure p_{nb}/p_c within the closed wake remains constant (Fig. 3c).

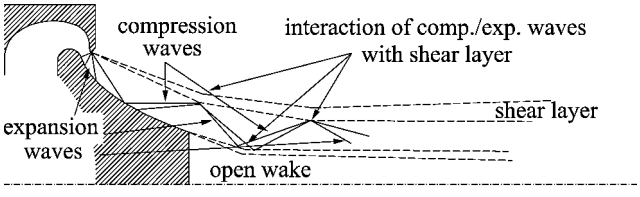

a) Underexpanded condition

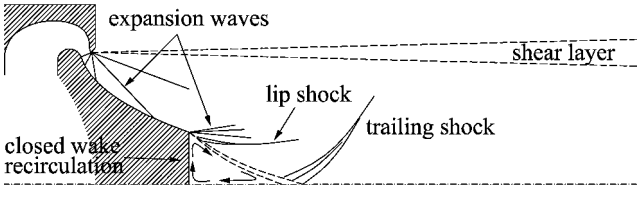

b) Design condition

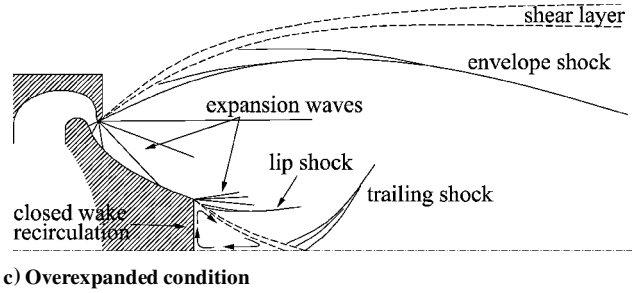

c) Overexpanded condition

Fig. 3 Flow phenomena of a truncated plug at different pressure ratios p_c/p_∞.

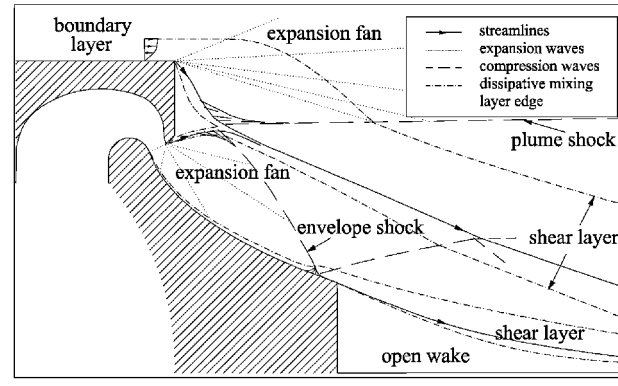

a) Open-nozzle base wake

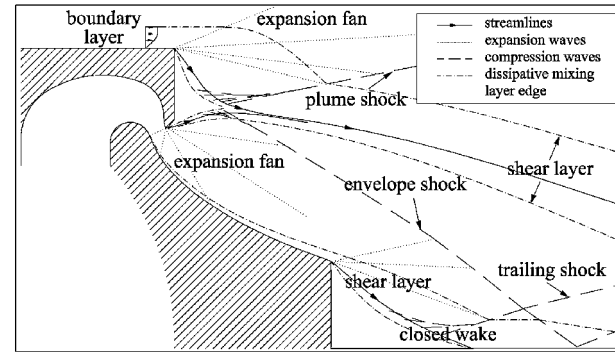

b) Closed-nozzle base wake

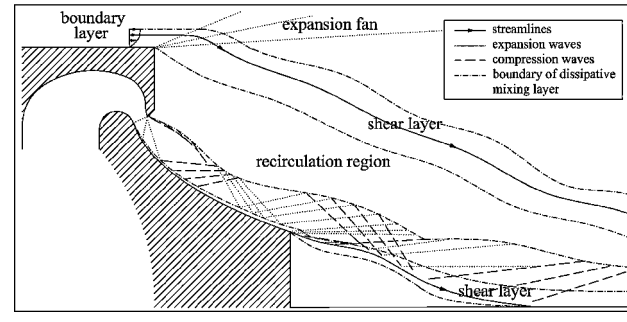

c) Open-vehicle base wake

Fig. 4 Flow phenomena with supersonic external flow.

External Flow Effects

The aspect of external flow effects will now be taken into account. The conditions at transonic and low supersonic external flow will be considered because of its dramatic influence on the decrease in thrust performance. This performance loss is primarily caused by the local flow phenomena in the vehicle base region around the vehicle aft end.[2]

The external freestream expands around the vehicle base to a pressure p_{vb}, which is much lower than the external flow pressure. Initially, the exhaust jet overexpands to this low pressure and moves outward. Farther downstream, where the ambient pressure is higher, the jet is turned inward. Inside the jet, this generates compression waves that coalesce into the envelope shock. The shock eventually impinges on the plug ramp (Fig. 4a) or downstream of the plug base. For high pressure ratios p_c/p_∞, the envelope shock may have passed the subsonic region of the wake (Fig. 4b). Then the base flow is insensitive to the ambient pressure (closed wake).

These two situations appear when the vehicle base wake is closed because the jet and the external flow cannot be kept separated by an open vehicle base wake. For low increasing pressure ratios, however, the vehicle base wake can be kept open[6] (Fig. 4c). This favorable condition will be further exploited when introducing the ventilated trailing-edge cavity afterbody.

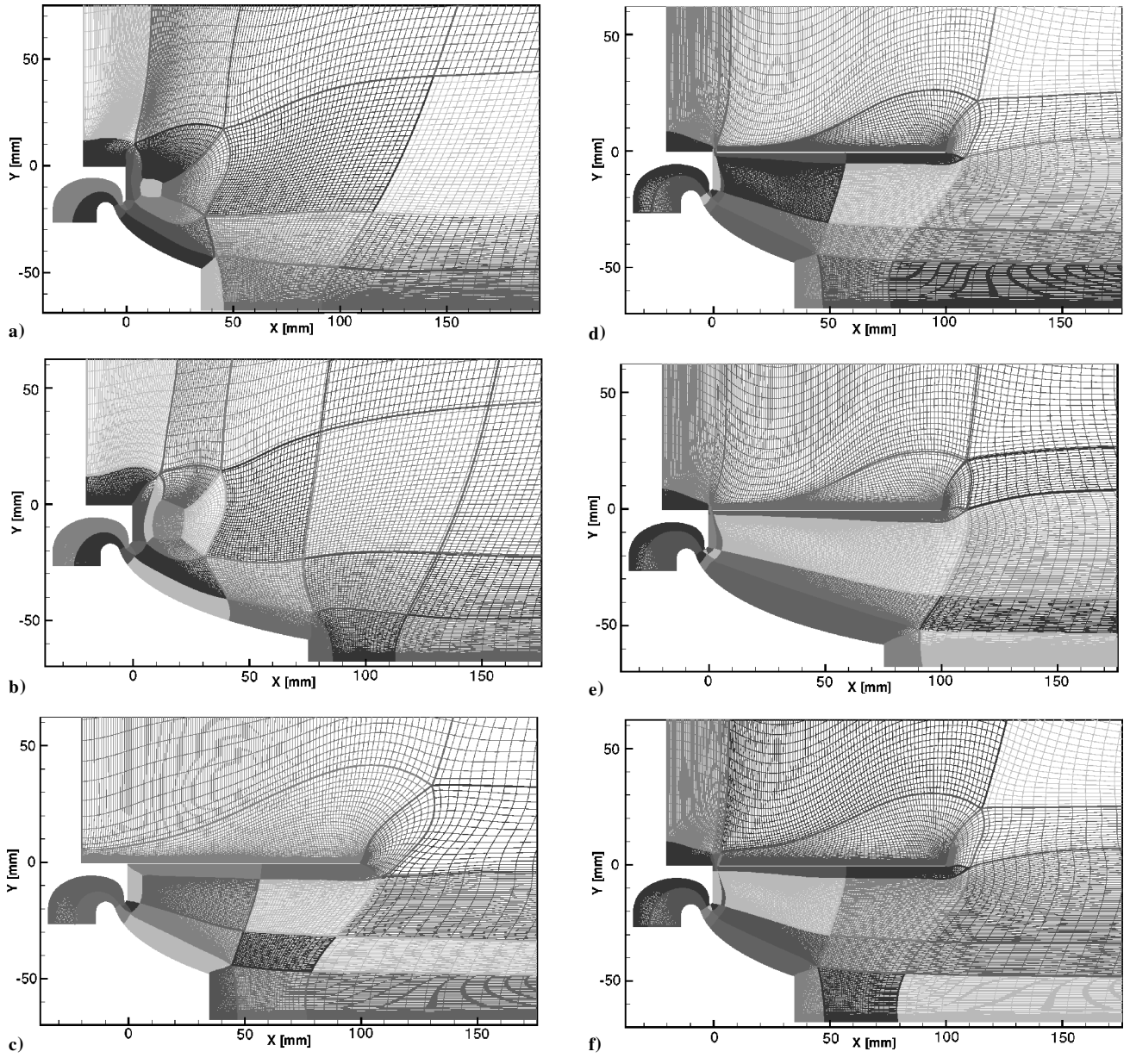

Fig. 5 Grid geometries of all models with corresponding number of grid cells: a) model 1 (47,566 grid cells), b) model 2 (44,890 grid cells), c) model 3 (72,894 grid cells), d) model 4 (71,332 grid cells), e) model 5 (69,682 grid cells), and f) model 6 (71,322 grid cells).

Description of Computations

The flow around the plug nozzle geometries is assumed to be two dimensional. The structured grids of all models are shown in Fig. 5, with their corresponding number of grid cells. Grid convergence has been proven by means of a comparison between calculations with these refined grids with course grids and with medium grids for a freestream Mach number of $M_\infty = 2$ and a pressure ratio of $p_c/p_\infty = 31.2$. For model 2 (Fig. 6), it has already been proven in our previous investigation.[6] The resulting drag coefficient of the entire nozzle C_D differed between the course grid and the medium grid by 2.6% and between the medium grid and the refined grid by only 0.036%. Also further enlargement of the lower tunnel wall did not produce significant variation in the results. Therefore, the number of grid points were found to be sufficient for the remainder of the cases studied. This results in a grid in which the supersonic inflow has been modeled up to $Y = 250$ mm and the outflow up to $X = 433$ mm. For the other models, it was assumed that the last refinement would result in differences in the drag coefficient of no less than $C_D = 0.1\%$. To prevent a subsonic area from entering the outflow of the grid, models 3–6 have been extended up to $X = 833$ mm.

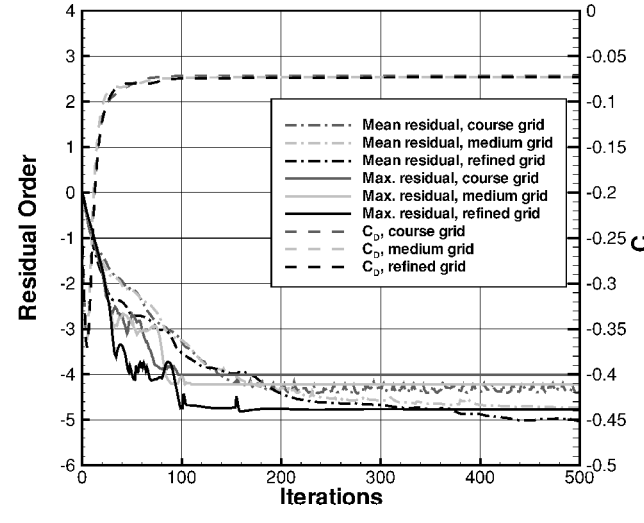

Fig. 6 Grid convergence of model 2 with $p_c/p_\infty = 31.2$ and $M_\infty = 2$.

To simulate the $\delta = 5.45$ mm boundary layer of the external flow, a Blasius profile for compressible flow was imposed on the inflow plane, corresponding to a boundary-layer thickness found earlier in wind-tunnel experiments.[6] The effect on the flow characteristics of having a full model was simulated by means of a symmetry plane.

Calculations on the geometries have been performed with $M_\infty = 2$, $T_t = 278$ K, and $p_{t_\infty} = 4.1$ bar. In several cases, it appeared to be very important whether the pressure ratio was increasing or decreasing. Therefore, calculations were started from results that would physically occur earlier in time. The pressure ratios were varying from $p_c/p_\infty = 3.5$ to 500. Turbulence have been simulated by means of a Baldwin–Lomax[16] turbulence closure model with a Degani–Schiff[17] correction.

Results

The results of the models are divided in two subsections. In the first, the differences in performance of the 20% model and its equivalents with a trailing-edge cavity of 100 mm and with single slits of 0, 1, and 2 mm are discussed. The second subsection deals with the comparison between the 20 and 40% model.

Ventilated Trailing-Edge Cavity

The favorable condition of an open vehicle base wake in the case of low-pressure ratios for a classical 20% plug nozzle has been further exploited by means of a ventilated trailing edge cavity (VTEC). The purpose of such a VTEC is to keep the external flow and the exhaust jet separated from each other up to higher pressure ratios, thereby, increasing the vehicle base pressure and restoring the altitude adaptive capabilities of the plug nozzle. In this subsection, the usefulness of such a system will be proven.

Because the exhaust jet adapts to the vehicle base pressure, this pressure is a good gauge for the performance of the models. We hereby negelect the additional drag caused by the VTEC. Figure 7 shows the vehicle base pressures vs the increasing and decreasing pressure ratio. It shows that the VTECs perform the best of the models. The trailing-edge cavity without slit can also keep its vehicle base wake open for higher pressure ratios (until $p_c/p_\infty = 20.7 - 31.2$), just like the VTEC with a 1-mm slit, but the vehicle base closed-wake performance is terrible. The VTECs, on the other hand, have essentially the same closed-wake performance as the classical 20% model, but the vehicle base hysteresis is shifted to higher pressure ratios. Because of the ventilation slits, the opening of the vehicle base wake for decreasing pressure ratio even increased to $p_c/p_\infty = 7.2 - 14.5$, thereby reducing its dependence on increasing or decreasing pressure ratios. The VTEC with the 2-mm slit retains its open vehicle base wake state for the highest

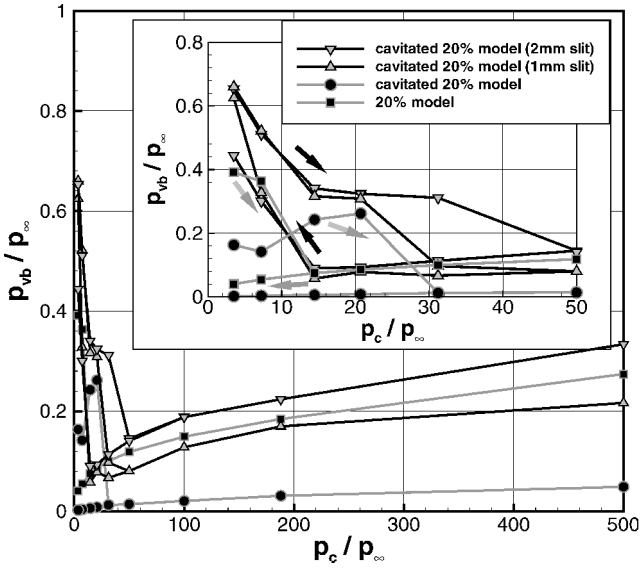

Fig. 7 Mean vehicle base pressure vs pressure ratio; 20% plug nozzle and $M_\infty = 2$.

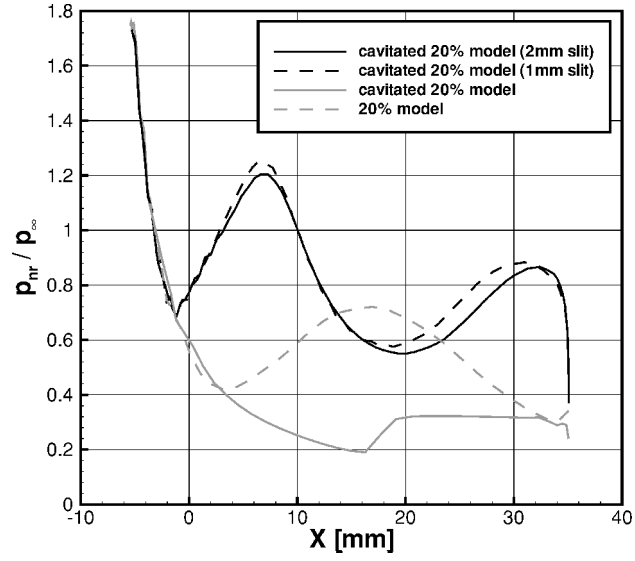

Fig. 8 Nozzle ramp pressure distribution with increasing $p_c/p_\infty = 3.5$; 20% plug nozzle and $M_\infty = 2$.

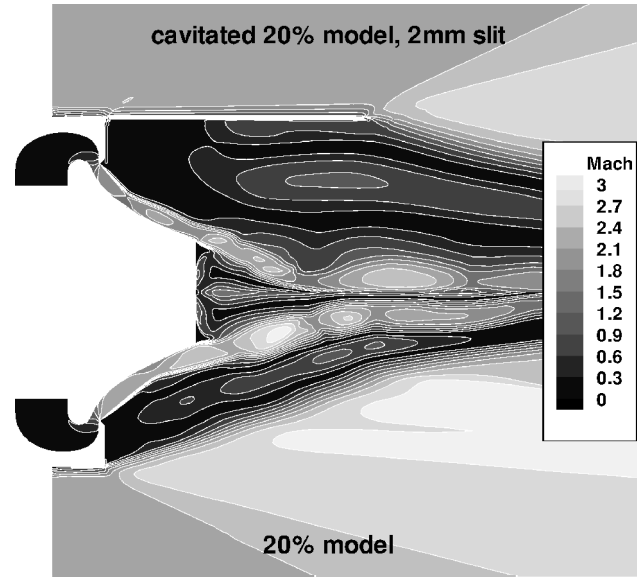

Fig. 9 Mach plot of 20% models with increasing pressure ratio; $p_c/p_\infty = 3.5$ and $M_\infty = 2$.

pressure ratio ($p_c/p_\infty = 31.2 - 50$). For higher pressure ratios, the performance of the trailing-edge cavities increases with increasing slit size, but only the 2-mm slit performs for these high pressure ratios better than the classical 20% model.

In Fig. 8, the nozzle ramp pressure distribution is presented for $p_c/p_\infty = 3.5$. It clearly shows that the high vehicle base pressures, found for the VTECs, are indeed a good gauge for high-pressure distributions along the nozzle ramp. The system of expansion and compression waves are responsible for the decreasing and increasing ramp pressures, respectively. A Mach plot showing this phenomenon for the normal 20% model and its equivalent with the VTEC and 2-mm slit is presented in Fig. 9.

The corresponding nozzle base pressures are presented in Fig. 10. For the normal 20% model, the closure of the nozzle base wake has been reached when the envelope shock has passed the region of the subsonic wake ($p_c/p_\infty = 20.7 - 31.2$). For the other models with trailing edge cavities, there is no envelope shock, which leads to relatively low nozzle base pressures between $p_c/p_\infty = 7.2$ and 31.2. The wake closes when the last right running characteristic of the Prandtl–Meyer expansion passes the subsonic region. For these closed-nozzle base wakes, the nozzle base pressures are practically equal.

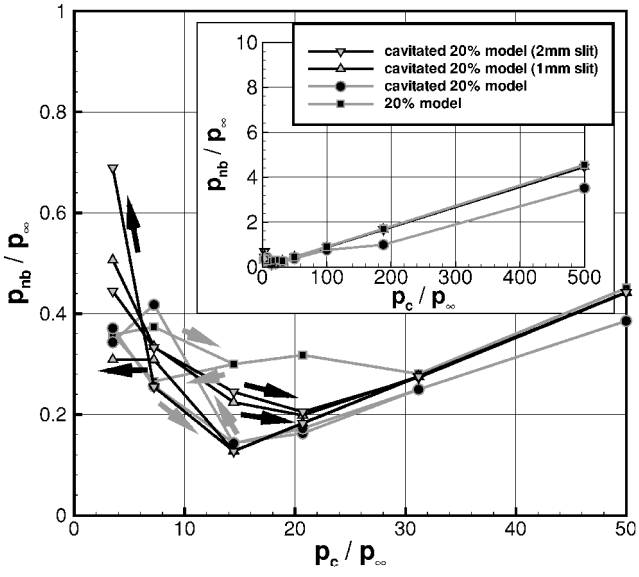

Fig. 10 Mean nozzle base pressure vs pressure ratio; 20% plug nozzle and $M_\infty = 2$.

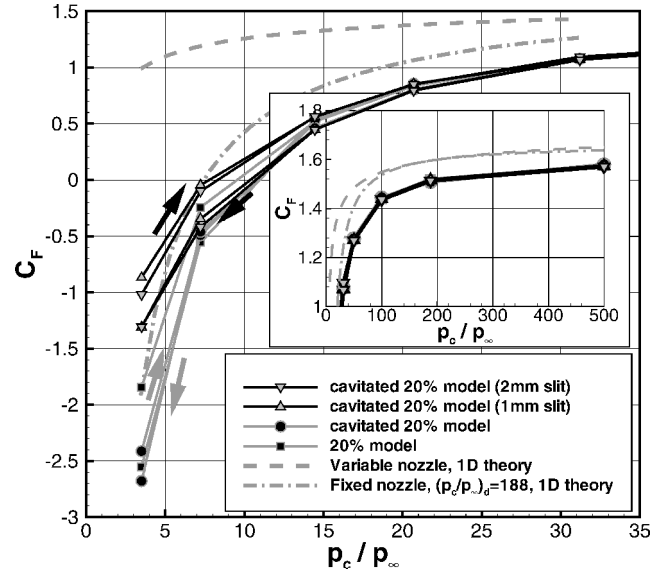

Fig. 11 Thrust coefficient vs pressure ratio; 20% plug nozzle and $M_\infty = 2$.

The contribution of all parts of the plug nozzle models to the total thrust are compared with each other, to that of an ideal, variable geometry bell nozzle, and to the thrust of a fixed nozzle with a design pressure ratio of $p_c/p_\infty = 188$. The thrust coefficient C_F is defined as the ratio of thrust over the jet stagnation pressure p_c acting on the sonic throat area A^* (Ref. 2):

$$C_F = F \Big/ p_c A^* \tag{1}$$

For an ideal nozzle with fixed geometry, thrust coefficient is given by the following equation:

$$C_{F_{\text{fixed}}} = \gamma M_d \sqrt{\left(\frac{2}{\gamma+1}\right)^{(\gamma+1)/(\gamma-1)} \left[1 \Big/ \left(1 + \frac{\gamma-1}{2} M_d^2\right)\right]} + \frac{A_d}{A^*}\left(\left\{1 \Big/ \left[\left(1 + \frac{\gamma-1}{2} M_d^2\right)^{\gamma/(\gamma-1)}\right]\right\} - \frac{p_\infty}{p_c}\right) \tag{2}$$

For the ideal nozzle with variable geometry the thrust coefficient equation becomes

$$C_{F_{\text{variable}}} = \gamma M_e \sqrt{\left(\frac{2}{\gamma+1}\right)^{(\gamma+1)/(\gamma-1)} \left[1 \Big/ \left(1 + \frac{\gamma-1}{2} M_e^2\right)\right]} \tag{3}$$

The thrust coefficient for the plug nozzle has been calculated by a discretized integration of the static pressures along its surfaces:

$$C_{F_{\text{plug}}} = \frac{1}{A^*} \int^{\text{surface}} \frac{p - p_\infty}{p_c} \, \mathrm{d}z \tag{4}$$

The corresponding thrust coefficients are shown in Fig. 11. The VTEC gives a dramatic rise in performance for the low-pressure ratios. For high-pressure ratios, there is almost no difference in the performances of the models, although the VTEC with the 2-mm slit performs slightly better than the rest. Therefore, one may conclude that VTECs are certainly an option for optimizing the plug nozzle performance. One has to be cautious to generalize this statement for all plug nozzle configurations, although this tool seems to be promising.

Plug Truncation

Subject of investigation has also been the differences in plug truncation for different afterbodies. Therefore, the classical 20% plug nozzle and the 20% plug nozzle with VTEC and 1-mm slit have been compared with their 40% equivalents. Figure 12 shows the vehicle base pressure vs pressure ratio for these models. For low pressure ratios, the performances of both the 20 and 40% models are essentially the same, although the 20% model shows slightly higher pressures. For high pressure ratios, the 20% model with VTEC and 1-mm slit shows, as mentioned before, lower vehicle base pressures than the classical 20% model. For the 40% model, on the other hand, the VTEC with 1-mm slit already shows higher vehicle base pressures than the classical 40% model. When comparing the VTEC models, the 40% model now shows the highest vehicle base pressures.

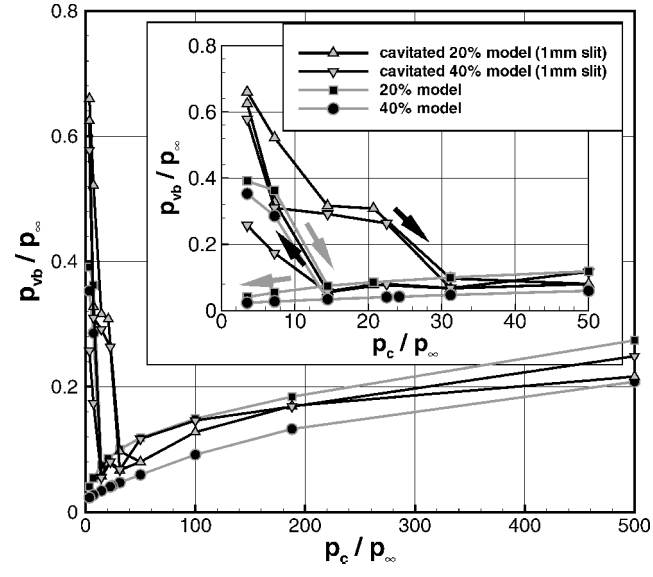

Fig. 12 Mean vehicle base pressure vs pressure ratio; 20 and 40% plug nozzle and $M_\infty = 2$.

The thrust coefficients of these models are presented in Fig. 13. For the low pressure ratios, the models with VTECs show much better performances. For high pressure ratios, these differences are almost negligible, but the differences between the 20 and 40% models cannot be neglected. The 40% model performs much better, but this is the price one has to pay for saving mass because of the truncation.

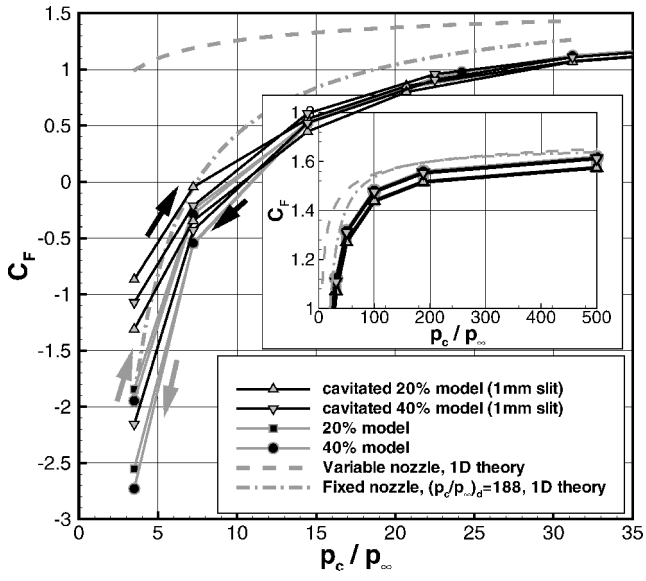

Fig. 13 Thrust coefficient vs pressure ratio; 20 and 40% plug nozzle and $M_\infty = 2$.

Conclusions

Comparison of the 20% model with VTEC and the original model shows that such an afterbody improves the plug nozzle performance, at least for the configurations tested. There is, however, no indication that this would not be the case for other configurations. For the widest slit, the open vehicle base wake can be kept open for higher pressure ratios. The same model has also the highest vehicle base pressures in the closed-wake state, resulting in the overall best performance.

Different plug truncations do not give qualitative different results, although the 20% VTEC model shows slightly better results in the low pressure ratios, and the 40% VTEC model gives much better results for high pressure ratios. These differences are, however, not caused by external flow effects.

For further optimization of a plug nozzle with a VTEC, enlargement of the ventilated region with multiple slits must be realized.

References

[1]Hagemann, G., Immich, H., Nguyen, T. V., and Dumnov, G. E., "Advanced Rocket Nozzles," *Journal of Propulsion and Power*, Vol. 14, No. 5, 1998, pp. 620–634.

[2]Ruf, J. H., and McConnaughey, P. K., "The Plume Physics Behind Aerospike Nozzle Altitude Compensation and Slipstream Effect," AIAA Paper 97-3218, July 1997.

[3]Immich, H., and Caporicci, M., "Status of the FESTIP Rocket Propulsion Technology Program," AIAA Paper 97-3311, July 1997.

[4]Hagemann, G., Schley, C.-A., Odintsov, E., and Sobatchkine, A., "Nozzle Flow Field Analysis with Particular Regard to 3D-Plug-Cluster Configurations," AIAA Paper 96-2954, July 1996.

[5]Rommel, T., Hagemann, G., Schley, C.-A., Manski, D., and Krülle, G., "Plug Nozzle Flowfield Analysis," *Journal of Propulsion and Power*, Vol. 13, No. 5, 1997, pp. 629–634.

[6]Wisse, M. E. N., and Bannink, W. J., "Half Model Restrictions for Linear Plug Nozzle Testing," *AIAA Journal*, Vol. 39, No. 11, 2001, pp. 2148–2157.

[7]Bannink, W. J., Schoones, M. M. J., and Houtman, E. M., "Experimental Study on the Interaction between Linear Plug Nozzle Exhaust Flow and Supersonic External Flow," *Proceedings of the Third European Symposium on Aerothermodynamics for Space Vehicles*, SP-426-1999, ESA, Noordwijk, The Netherlands, 1999, pp. 403–410.

[8]Muylaert, J., and Schwane, R., *Proceedings of the Second Workshop on Plug Nozzle Flow Validation*, MPA2446/RS, ESA, Noordwijk, The Netherlands, 1999.

[9]Hagemann, G., Immich, H., and Terhardt, M., "Flow Phenomena in Advanced Rocket Nozzles—The Plug Nozzle," AIAA Paper 98-3522, July 1998.

[10]Nasuti, F., and Onofri, M., "A Methodology to Solve Flowfields of Plug Nozzles for Future Launchers," *Journal of Propulsion and Power*, Vol. 14, No. 3, 1998, pp. 318–326.

[11]Immich, H., Nasuti, F., Onofri, M., and Caporicci, M., "Experimental and Numerical Analysis of Linear Plug Nozzles," AIAA Paper 98-1603, July 1998.

[12]Wasko, R. A., "Performance of Annular Plug and Expansion-Deflection Nozzles Including External Flow Effects at Transonic Mach Numbers," NASA TN-D-4462, 1968.

[13]Nash, J. F., "A Discussion of Two-Dimensional Turbulent Base Flows," Aeronautical Research Council, Rept. and Memoranda 3468, London, July 1965.

[14]Angelino, G., "Approximate Method for Plug Nozzle Design," *AIAA Journal*, Vol. 2, No. 10, 1964, pp. 1834, 1835.

[15]Houtman, E. M., "Numerical Simulation of Three-Dimensional Compressible Flows," Dept. of Aerospace Engineering, Rept. HSL TM 960381, Delft Univ. of Technology, Delft, The Netherlands, Nov. 1996.

[16]Baldwin, B. S., and Lomax, H., "Thin Layer Approximation and Algebraic Model for Separated Turbulent Flows," AIAA Paper 78-0257, Jan. 1978.

[17]Degani, D., and Schiff, L. B., "Computation of Turbulent Supersonic Flows Around Pointed Bodies Having Crossflow Separation," *Journal of Computational Physics*, Vol. 66, No. 1, 1986, pp. 173–196.

I. Gokalp
Associate Editor